

Ultrafast Intersystem Crossing and Spin Dynamics of Photoexcited Perylene-3,4:9,10-bis(dicarboximide) Covalently Linked to a Nitroxide Radical at Fixed Distances

Emilie M. Giacobbe, Qixi Mi, Michael T. Colvin, Boiko Cohen, Charusheela Ramanan, Amy M. Scott, Sina Yeganeh, Tobin J. Marks,* Mark A. Ratner,* and Michael R. Wasielewski*

Department of Chemistry, Argonne-Northwestern Solar Energy Research (ANSER) Center, and International Institute for Nanotechnology, Northwestern University, Evanston, Illinois 60208-3113

Received November 13, 2008; E-mail: m-wasielewski@northwestern.edu

Abstract: Time-resolved transient optical absorption and EPR (TREPR) spectroscopies are used to probe the interaction of the lowest excited singlet state of perylene-3,4:9,10-bis(dicarboximide) (^1PDI) with a stable *tert*-butylphenylnitroxide radical ($^2\text{BPNO}^*$) at specific distances and orientations. The $^2\text{BPNO}^*$ radical is connected to the PDI with the nitroxide and imide nitrogen atoms either para (**1**) or meta (**3**) to one another, as well as through a second intervening *p*-phenylene spacer (**2**). Transient absorption experiments on **1–3** reveal that ^1PDI undergoes ultrafast enhanced intersystem crossing and internal conversion with $\tau \approx 2$ ps to give structurally dependent 8–31% yields of ^3PDI . Energy- and electron-transfer quenching of ^1PDI by $^2\text{BPNO}^*$ are excluded on energetic and spectroscopic grounds. TREPR experiments at high magnetic fields (3.4 T, 94 GHz) show that the photogenerated three-spin system consists of the strongly coupled unpaired electrons confined to ^3PDI , which are each weakly coupled to the unpaired electron on $^2\text{BPNO}^*$ to form excited doublet (D_1) and quartet (Q) states, which are both spectrally resolved from the $^2\text{BPNO}^*$ (D_0) ground state. The initial spin polarizations of D_1 and Q are emissive for **1** and **2** and absorptive for **3**, which evolve over time to the opposite spin polarization. The subsequent decays of D_1 and Q to ground-state spin polarize D_0 . The rates of polarization transfer depend on the molecular connectivity between PDI and $^2\text{BPNO}^*$ and can be rationalized in terms of the dependence on molecular structure of the through-bond electronic coupling between these species.

Introduction

Controlling the spin dynamics of complex multispin systems is a major goal in the quest for molecule-based spintronics.^{1–4} Photoexcitation of organic molecules has been shown to control their properties in a wide variety of photonics applications,^{5–10} while modern electron paramagnetic resonance (EPR) techniques provide an important avenue for manipulating spin systems.^{11–14}

Photoexcitation can produce well-defined initial spin states; for example, spin-selective intersystem crossing following photoexcitation often produces highly spin-polarized triplet states.¹⁵ The interaction of these triplet states with stable radicals often results in electron spin polarization of the radical, providing a facile means for introducing and controlling spin polarization in organic materials.^{16–22} A second strategy uses photoinitiated ultrafast electron transfer within covalently linked organic donor–acceptor molecules having specific donor–acceptor distances and orientations to produce highly spin-polarized radical

- (1) Rajca, A. *Adv. Phys. Org. Chem.* **2005**, *40*, 153–199.
- (2) Epstein, A. J. *MRS Bull.* **2003**, *28*, 492–499.
- (3) Awschalom, D. D.; Flatte, M. E.; Samarth, N. *Sci. Am.* **2002**, *286*, 67–73.
- (4) Wolf, S. A.; Awschalom, D. D.; Buhman, R. A.; Daughton, J. M.; von Molnar, S.; Roukes, M. L.; Chtchelkanova, A. Y.; Treger, D. M. *Science* **2001**, *294*, 1488–1495.
- (5) Wasielewski, M. R. *J. Org. Chem.* **2006**, *71*, 5051–5066.
- (6) Verhoeven, J. W. *J. Photochem. Photobiol. C* **2006**, *7*, 40–60.
- (7) Segura, J. L.; Martin, N.; Guldi, D. M. *Chem. Soc. Rev.* **2005**, *34*, 31–47.
- (8) Holten, D.; Bocian, D. F.; Lindsey, J. S. *Acc. Chem. Res.* **2002**, *35*, 57–69.
- (9) Lukas, A. S.; Wasielewski, M. R. In *Molecular Switches*; Feringa, B. L., Ed.; Wiley-VCH: Weinheim, 2001; pp 1–35.
- (10) de Silva, A. P.; Guanaratne, H. Q. N.; Gunnlaugsson, T.; Huxley, A. J. M.; McCoy, C. P.; Rademacher, J. T.; Rice, T. E. *Chem. Rev.* **1997**, *97*, 1515–1566.
- (11) Mehring, M.; Mende, J. *Phys. Rev. A: At., Mol., Opt. Phys.* **2006**, *73*, 052303/052301 052303/052312.
- (12) Harnett, W. *Phys. Rev. A* **2002**, *65*, 032322.

- (13) Jones, J. A. In *The physics of quantum information*; Bouwmeester, D., Ekert, A., Zeilinger, A., Eds.; Springer: Berlin, 2000; pp 177–189.
- (14) Schweiger, A.; Jeschke, G. *Principles of pulsed electron paramagnetic resonance*; Oxford: Oxford, 2001.
- (15) Levanon, H.; Norris, J. R. *Chem. Rev.* **1978**, *78*, 185–198.
- (16) Kawai, A.; Shibuya, K. *J. Photochem. Photobiol., C* **2006**, *7*, 89–103.
- (17) Franco, L.; Mazzoni, M.; Corvaja, C.; Gubskaya, V. P.; Berezhnaya, L. S.; Nuretdinov, I. A. *Mol. Phys.* **2006**, *104*, 1543–1550.
- (18) Rozenshtein, V.; Berg, A.; Stavitski, E.; Levanon, H.; Franco, L.; Corvaja, C. *J. Phys. Chem. A* **2005**, *109*, 11144–11154.
- (19) Blank, A.; Levanon, H. *Mol. Phys.* **2002**, *100*, 1477–1488.
- (20) Sartori, E.; Toffoletti, A.; Corvaja, C.; Garlaschelli, L. *J. Phys. Chem. A* **2001**, *105*, 10776–10780.
- (21) Blank, A.; Levanon, H. *J. Phys. Chem. A* **2001**, *105*, 4799–4807.
- (22) Fujisawa, J.; Ishii, K.; Ohba, Y.; Yamauchi, S.; Fuhs, M.; Möbius, K. *J. Phys. Chem. A* **1999**, *103*, 213–216.

pairs (RPs) in which the initial spin state is well defined.^{23–27} We and others investigated how to control the spin dynamics of these covalent RPs using the influence of additional spins.^{28–35} These organic RPs display coherent spin motion for microseconds at room temperature and longer at low temperatures,^{36,37} which makes it possible that this coherence could provide the basis for new organic information-processing devices.^{3,35,38–42}

Spin polarization as a result of triplet–radical interactions has been attributed for the most part to two complementary mechanisms, the radical–triplet pair mechanism (RTPM)^{22,43–56}

and electron spin polarization transfer (ESPT).^{21,50,65} A triplet state with a Boltzmann population of its spin sublevels can polarize a radical by means of a spin-sorting process. Both mechanisms are predicated on diffusive encounters between the photoexcited triplet state molecule and the radical in solution. In the case of the RTPM, however, it is not necessary for the triplet state to be polarized initially. Recently, a few examples of photoexcited triplet states having covalently attached radicals have appeared, e.g., ZnTPP coordinated with pyridylnitronyl nitroxides^{22,53,54,57} and *tert*-butylpyridyl nitroxides,^{58,59} silicon phthalocyanines and fullerenes with attached 2,2,6,6-tetramethylpiperidine-*N*-oxyl (TEMPO) substituents,^{18,20,60–64} as well as verdazyl and nitronyl nitroxides attached to polycyclic aromatic molecules.^{65–69}

In many of these systems there is an ambiguity as to whether the initial triplet state of the chromophore arises from normal spin–orbit-induced intersystem crossing (SO-ISC) or whether it results from a direct interaction of the radical spin with the lowest excited singlet state of the chromophore. Quenching of fluorescent chromophores by stable radicals has been extensively studied in a wide variety of noncovalent and flexibly linked covalent systems.^{70–82} However, there are very few examples of rigid systems in which the structural and electronic basis of

- (23) Hasharoni, K.; Levanon, H.; Greenfield, S. R.; Gosztola, D. J.; Svec, W. A.; Wasielewski, M. R. *J. Am. Chem. Soc.* **1995**, *117*, 8055–8056.
- (24) Carbonera, D.; DiValentin, M.; Corvaja, C.; Agostini, G.; Giacometti, G.; Liddell, P. A.; Kuciauskas, D.; Moore, A. L.; Moore, T. A.; Gust, D. *J. Am. Chem. Soc.* **1998**, *120*, 4398–4405.
- (25) Weiss, E. A.; Ratner, M. A.; Wasielewski, M. R. *J. Phys. Chem. A* **2003**, *107*, 3639–3647.
- (26) Weiss, E. A.; Ahrens, M. J.; Sinks, L. E.; Gusev, A. V.; Ratner, M. A.; Wasielewski, M. R. *J. Am. Chem. Soc.* **2004**, *126*, 5577–5584.
- (27) Dance, Z. E. X.; Mi, Q. X.; McCamant, D. W.; Ahrens, M. J.; Ratner, M. A.; Wasielewski, M. R. *J. Phys. Chem. B* **2006**, *110*, 25163–25173.
- (28) Chernick, E. T.; Mi, Q.; Vega, A. M.; Lockard, J. V.; Ratner, M. A.; Wasielewski, M. R. *J. Phys. Chem. B* **2007**, *111*, 6728–6737.
- (29) Mi, Q.; Chernick, E. T.; McCamant, D. W.; Weiss, E. A.; Ratner, M. A.; Wasielewski, M. R. *J. Phys. Chem. A* **2006**, *110*, 7323–7333.
- (30) Chernick, E. T.; Mi, Q.; Kelley, R. F.; Weiss, E. A.; Jones, B. A.; Marks, T. J.; Ratner, M. A.; Wasielewski, M. R. *J. Am. Chem. Soc.* **2006**, *128*, 4356–4364.
- (31) Ishii, K.; Hirose, Y.; Kobayashi, N. *J. Phys. Chem. A* **1999**, *103*, 1986–1990.
- (32) Mori, Y.; Sakaguchi, Y.; Hayashi, H. *J. Phys. Chem. A* **2000**, *104*, 4896–4905.
- (33) Mori, Y.; Sakaguchi, Y.; Hayashi, H. *Bull. Chem. Soc. Jpn.* **2001**, *74*, 293–304.
- (34) Vlasiouk, I.; Smirnov, S.; Kutzki, O.; Wedel, M.; Montforts, F.-P. *J. Phys. Chem. B* **2002**, *1–6*, 8657–8666.
- (35) Buchachenko, A. L.; Berdinsky, V. L. *Chem. Rev.* **2002**, *102*, 603–612.
- (36) Prisner, T.; Dobbert, O.; Dinse, K. P.; van Willigen, H. *J. Am. Chem. Soc.* **1988**, *110*, 1622–1623.
- (37) Angerhofer, A.; Toporowicz, M.; Bowman, M. K.; Norris, J. R.; Levanon, H. *J. Phys. Chem.* **1988**, *92*, 7164–7166.
- (38) Lahti, P. M., Ed.; *Magnetic Properties of Organic Materials*; Dekker: New York, 1999.
- (39) Sugawara, T.; Sakurai, H.; Izuoka, A., Eds. *Electronically controllable high spin systems realized by spin-polarized donors*; Gordon and Breach: Amsterdam, 2001.
- (40) Miller, J. S.; Manson, J. L. *Acc. Chem. Res.* **2001**, *34*, 563–570.
- (41) Rajca, A. *Chem. Eur. J.* **2002**, *8*, 4834–4841.
- (42) Itkis, M. E.; Chi, X.; Cordes, A. W.; Haddon, R. C. *Science* **2002**, *296*, 1443–1445.
- (43) Blättler, C.; Jent, F.; Paul, H. *Chem. Phys. Lett.* **1990**, *166*, 375–380.
- (44) Jenks, W. S.; Turro, N. J. *Res. Chem. Intermed.* **1990**, *13*, 237.
- (45) Kawai, A.; Okutsu, T.; Obi, K. *J. Phys. Chem.* **1991**, *95*, 9130–9134.
- (46) Kawai, A.; Obi, K. *J. Phys. Chem.* **1992**, *96*, 52–56.
- (47) Turro, N. J.; Khudyakov, I. V.; Bossmann, S. H.; Dwyer, D. W. *J. Phys. Chem.* **1993**, *97*, 1138–1146.
- (48) Goudsmit, G. H.; Paul, H.; Shushin, A. I. *J. Phys. Chem.* **1993**, *97*, 13243–13249.
- (49) Corvaja, C.; Franco, L.; Toffoletti, A. *Appl. Magn. Reson.* **1994**, *7*, 257–269.
- (50) Fujisawa, J.; Ishii, K.; Ohba, Y.; Iwaizumi, M.; Yamauchi, S. *J. Phys. Chem.* **1995**, *99*, 17082–17084.
- (51) Hugerat, M.; van der Est, A.; Ojadi, E.; Biczok, L.; Linschitz, H.; Levanon, H.; Stehlik, D. *J. Phys. Chem.* **1996**, *100*, 495–500.
- (52) Regev, A.; Galili, T.; Levanon, H. *J. Phys. Chem.* **1996**, *100*, 18502–18510.
- (53) Ishii, K.; Fujisawa, J.; Ohba, Y.; Yamauchi, S. *J. Am. Chem. Soc.* **1996**, *118*, 13079–13080.
- (54) Fujisawa, J.; Ishii, K.; Ohba, Y.; Yamauchi, S.; Fuhs, M.; Möbius, K. *J. Phys. Chem. A* **1997**, *101*, 5869–5876.
- (55) Fujisawa, J.; Ohba, Y.; Yamauchi, S. *J. Phys. Chem. A* **1997**, *101*, 434–439.
- (56) Fujisawa, J.; Ohba, Y.; Yamauchi, S. *Chem. Phys. Lett.* **1998**, *294*, 248–254.
- (57) Fujisawa, J.; Ishii, K.; Ohba, Y.; Yamauchi, S.; Fuhs, M.; Möbius, K. *J. Phys. Chem. A* **1999**, *103*, 3138.
- (58) Tarasov, V. F.; Saiful, I. S. M.; Iwasaki, Y.; Ohba, Y.; Savitsky, A.; Möbius, K.; Yamauchi, S. *Appl. Magn. Reson.* **2006**, *30*, 619–636.
- (59) Tarasov, V. F.; Saiful, I. S. M.; Ohba, Y.; Takahashi, K.; Yamauchi, S. *Spectrochim. Acta, Part A* **2008**, *69*, 1327–1330.
- (60) Ishii, K.; Hirose, Y.; Fujitsuka, H.; Ito, O.; Kobayashi, N. *J. Am. Chem. Soc.* **2001**, *123*, 702–708.
- (61) Takeuchi, S.; Ishii, K.; Kobayashi, N. *J. Phys. Chem. A* **2004**, *108*, 3276–3280.
- (62) Corvaja, C.; Franco, L.; Mazzoni, M. *Appl. Magn. Reson.* **2001**, *20*, 71–83.
- (63) Corvaja, C.; Maggini, M.; Prato, M.; Scorrano, G.; Venzin, M. *J. Am. Chem. Soc.* **1995**, *117*, 8857–8858.
- (64) Conti, F.; Corvaja, C.; Toffoletti, A.; Mizuochi, N.; Ohba, Y.; Yamauchi, S.; Maggini, M. *J. Phys. Chem. A* **2000**, *104*, 4962–4967.
- (65) Teki, Y.; Tamekuni, H.; Takeuchi, J.; Miura, Y. *Angew. Chem., Int. Ed.* **2006**, *45*, 4666–4670.
- (66) Teki, Y.; Kimura, M.; Narimatsu, S.; Ohara, K.; Mukai, K. *Bull. Chem. Soc. Jpn.* **2004**, *77*, 95–99.
- (67) Teki, Y.; Nakatsuji, M.; Miura, Y. *Mol. Phys.* **2002**, *100*, 1385–1394.
- (68) Teki, Y.; Miyamoto, S.; Nakatsuji, M.; Miura, Y. *J. Am. Chem. Soc.* **2001**, *123*, 294–305.
- (69) Teki, Y.; Miyamoto, S.; Imura, K.; Nakatsuji, M.; Miura, Y. *J. Am. Chem. Soc.* **2000**, *122*, 984–985.
- (70) Blough, N. V.; Simpson, D. J. *J. Am. Chem. Soc.* **1988**, *110*, 1915–1917.
- (71) Chattopadhyay, S. K.; Das, P. K.; Hug, G. L. *J. Am. Chem. Soc.* **1983**, *105*, 6205–6210.
- (72) Green, J. A.; Singer, L. A.; Parks, J. H. *J. Chem. Phys.* **1973**, *58*, 2690–2695.
- (73) Green, S. A.; Simpson, D. J.; Zhou, G.; Ho, P. S.; Blough, N. V. *J. Am. Chem. Soc.* **1990**, *112*, 7337–7346.
- (74) Herbelin, S. E.; Blough, N. V. *J. Phys. Chem. B* **1998**, *102*, 8170–8176.
- (75) Hrdlovic, P.; Chmela, S.; Sarakha, M.; Lacoste, J. J. *Photochem. Photobiol., A* **2001**, *138*, 95–109.
- (76) Karpiuk, J.; Grabowski, Z. R. *Chem. Phys. Lett.* **1989**, *160*, 451–456.
- (77) Kollar, J.; Hrdlovic, P.; Chmela, S.; Sarakha, M.; Guyot, G. *J. Photochem. Photobiol., A* **2005**, *170*, 151–159.
- (78) Kuz'min, V. A.; Tatikolov, A. S. *Chem. Phys. Lett.* **1977**, *51*, 45–47.
- (79) Likhtenstein, G. I.; Ishii, K.; Nakatsuji, S. *J. Photochem. Photobiol.* **2007**, *83*, 871–881.
- (80) Medvedeva, N.; Martin, V. V.; Weis, A. L.; Likhtenshten, G. I. *J. Photochem. Photobiol., A* **2004**, *163*, 45–51.
- (81) Sartori, E.; Toffoletti, A.; Corvaja, C.; Moroder, L.; Formaggio, F.; Toniolo, C. *Chem. Phys. Lett.* **2004**, *385*, 362–367.

the quenching has been studied, and in these systems only fluorescence quantum yields and lifetimes have been examined.^{31,53,60} Several photophysical mechanisms have been proposed to account for this quenching



where eq 1 is electron transfer, eq 2 is Förster and/or Dexter energy transfer, eq 3 is electron exchange induced enhanced intersystem crossing (EISC), and eq 4 is enhanced internal conversion (EIC). Electron transfer from a TEMPO free radical to the triplet state of a covalently linked 1,8:4,5-naphthalene-bis(dicarboximide) (NI) chromophore has been reported to occur with $\tau_{\text{cs}} < 15$ ns in acetonitrile, resulting in a long-lived charge-separated state with a lifetime of $>200 \mu\text{s}$.⁸³ Several studies have reported the oxidation of nitroxide radicals by fullerene triplet states, but they are limited to intermolecular interactions.^{84–86} Fluorescence quenching as a result of electron transfer to or from a stable radical has often been considered unlikely due to the lack of a solvent dependence, which is often key evidence for assigning this mechanism.⁷² However, it has been argued that a lack of solvent dependence is not definitive evidence for ruling out electron transfer, since the process could be diffusion controlled and not appear solvent dependent.⁷¹ It has yet to be conclusively demonstrated that the excited singlet state of a chromophore is quenched by electron transfer to or from a stable radical.

Fluorescence resonance energy transfer (FRET) is generally thought to be insignificant for nitroxide radicals as their optical transitions in the visible spectrum have very low oscillator strengths. Yet, exceptions have been proposed,⁸⁷ and when energy-accepting radicals are freely diffusing in solution, it is also necessary to consider the distribution of distances and presence of multiple radicals in the proximity of one energy donor.⁸⁸

EIC and EISC are the two most often cited mechanisms for excited singlet-state quenching by stable radicals. Quenching of the singlet state of fluorescamine dyes derivatized with nitroxides by EIC as monitored by transient absorption has been proposed.⁷⁴ The absence of fluorescamine triplet–triplet absorption features in the transient absorption spectrum and unfavorable energetics for energy transfer led the authors to conclude that EIC is the most likely quenching mechanism. The quench-

ing of the lowest excited singlet state of rubrene in the presence of 4-hydroxy-TEMPO has also been attributed to EIC, which was quite unexpected as many similar systems are quenched to form large triplet yields in the presence of TEMPO.⁸²

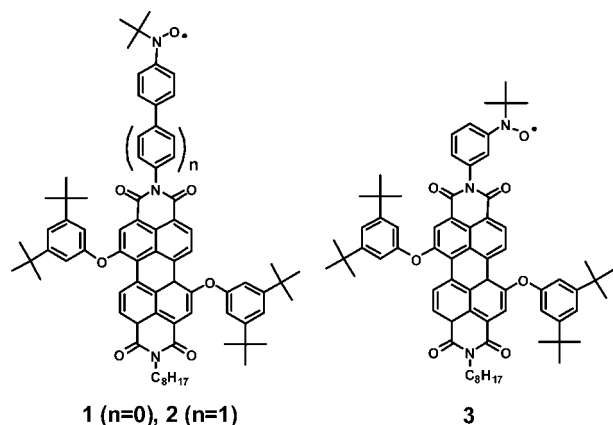
Intermolecular quenching of chromophore excited singlet states by EISC leads to enhanced triplet quantum yields in the presence of a radical.^{73,76–78,81} Intersystem crossing within a chromophore is normally a spin-forbidden process but can be accelerated by an organic free radical.^{35,89} Again, most of the work surrounding this idea is based on interactions of freely diffusing radicals and chromophores in solution; however, several studies of covalently linked chromophore–radical dyads have appeared, which seek to control to some degree the distances and orientations between the chromophore and the radical and thereby control their electronic interactions. Green et al.⁷³ studied a series of molecules in which TEMPO was covalently bound to naphthalene by a variety of covalent linkages and concluded that EISC via local relaxation of the singlet, not energy transfer, is the dominant mechanism for quenching. Intersystem crossing in the presence of TEMPO or structurally related derivatives has also been observed for a variety of aromatic hydrocarbons such as naphthalene and pyrene, phenanthrene, 1,2-benzanthrene, azulene from its S₂ state, and perylene, as indicated by an increase in triplet quantum yield.^{72,76,78,81} In all of these cases, the authors note that while EISC dominates, there may be other mechanisms contributing to the decay of the excited singlet states.

Perylene-3,4:9,10-bis(dicarboximide) (PDI) and its derivatives are robust organic dyes that strongly absorb visible light and display a strong tendency to self-assemble into ordered aggregates, thus generating significant interest as photoactive materials in a wide variety of organic electronics.^{90–98} PDI is both photochemically and thermally stable,⁹⁹ is easily functionalized, and serves as an excellent electron acceptor with a reversible reduction potential.¹⁰⁰ Moreover, PDI has a fluorescence quantum yield that is close to unity,¹⁰¹ so that it has a very low intrinsic triplet yield due to SO-ISC. If a stable radical is covalently linked to PDI at a fixed distance and ³PDI is formed by the interaction of ¹PDI with the stable radical, the dynamics of this process should be attributable exclusively to mechanisms other than normal SO-ISC, and this would provide an informative probe of how ³PDI formation depends on the structure and electronic properties of the PDI–radical system.

- (82) Yee, W. A.; Kuzmin, V. A.; Kliger, D. S.; Hammond, G. S.; Twarowski, A. J. *J. Am. Chem. Soc.* **1979**, *101*, 5104–5106.
 (83) Green, S.; Fox, M. A. *J. Phys. Chem.* **1995**, *99*, 14752–14757.
 (84) Araki, Y.; Luo, H.; Islam, S. D. M.; Ito, O.; Matsushita, M. M.; Iyoda, T. *J. Phys. Chem. A* **2003**, *107*, 2815–2820.
 (85) Borisevich, Y. E.; Kuz'min, V. A.; Renge, I. V.; Darmanyan, A. P. *Izv. Akad. Nauk SSSR, Ser. Khim.* **1981**, *201*, 4–2019.
 (86) Samanta, A.; Kamat, P. V. *Chem. Phys. Lett.* **1992**, *199*, 635–639.
 (87) Puskin, J. S.; Vistnes, A. I.; Coene, M. T. *Arch. Biochem. Biophys.* **1981**, *206*, 164–172.
 (88) Lakowicz, J. R. *Principles of Fluorescence Spectroscopy*; Kluwer: Dordrecht, 1999.

- (89) Hoytink, G. J. *Acc. Chem. Res.* **1969**, *2*, 114–120.
 (90) Tang, C. W. *App. Phys. Lett.* **1986**, *48*, 183–185.
 (91) Ford, W. E.; Kamat, P. V. *J. Phys. Chem.* **1987**, *91*, 6373–6380.
 (92) Ford, W. E.; Hiratsuka, H.; Kamat, P. V. *J. Phys. Chem.* **1989**, *93*, 6692–6696.
 (93) Würthner, F.; Thalacker, C.; Sautter, A. *Adv. Mater.* **1999**, *11*, 754–758.
 (94) Dittmer, J. J.; Marseglia, E. A.; Friend, R. H. *Adv. Mater.* **2000**, *12*, 1270–1274.
 (95) Langhals, H.; Saulich, S. *Chem. Eur. J.* **2002**, *8*, 5630–5643.
 (96) Gregg, B. A. *J. Phys. Chem. B* **2003**, *107*, 4688–4698.
 (97) Neuteboom, E. E.; Meskers, S. C. J.; Van Hal, P. A.; Van Duren, J. K. J.; Meijer, E. W.; Janssen, R. A. J.; Dupin, H.; Pourtois, G.; Cornil, J.; Lazzaroni, R.; Bredas, J.-L.; Beljonne, D. *J. Am. Chem. Soc.* **2003**, *125*, 8625–8638.
 (98) Han, J. J.; Shaller, A. D.; Wang, W.; Li, A. D. Q. *J. Am. Chem. Soc.* **2008**, *130*, 6974–6982.
 (99) Langhals, H.; Ismael, R. *Eur. J. Org. Chem.* **1998**, *191*, 5–1917.
 (100) Gosztola, D.; Niemczyk, M. P.; Svec, W. A.; Lukas, A. S.; Wasielewski, M. R. *J. Phys. Chem. A* **2000**, *104*, 6545–6551.
 (101) Giaimo, J. M.; Lockard, J. V.; Sinks, L. E.; Scott, A. M.; Wilson, T. M.; Wasielewski, M. R. *J. Phys. Chem. A* **2008**, *112*, 2322–2330.

In this paper, we present both ultrafast transient optical absorption studies and time-resolved EPR (TREPR) studies at high magnetic fields to probe the interaction of PDI with a stable *tert*-butylphenylnitroxide radical (${}^2\text{BPNO}^{\bullet}$). The ${}^2\text{BPNO}^{\bullet}$ radical is connected via its 4-position either directly to the PDI imide nitrogen (**1**) or to an intervening phenyl spacer (**2**). In addition, the BPNO $^{\bullet}$ radical is attached at its 3-position directly to the PDI imide nitrogen atom (**3**). The changes in radical–chromophore distance and orientation within **1–3** are used to probe how the interaction between them depends on electronic coupling.



Experimental Section

The syntheses and characterization of compounds **1–3** are described in detail in the Supporting Information. All reagents were purchased from Sigma-Aldrich and used as received. Triethylamine was distilled over CaH_2 prior to use. All final products were purified by normal-phase preparative thin layer chromatography prior to characterization. All solvents were spectrophotometric grade or distilled prior to use.

Electrochemical measurements were performed on a CH Instruments model 660A electrochemical workstation. All samples were measured in a solution of 0.1 M tetra-*n*-butylammonium hexafluorophosphate (TBAPF_6) in dichloromethane purged with N_2 to remove oxygen. A 1.0 mm diameter platinum disk electrode, platinum wire counter electrode, and silver wire reference electrode were used. The ferrocene/ferrocenium couple was used as an internal reference. Spectroelectrochemistry was performed in solutions of 0.1 M TBAPF_6 in butyronitrile using a platinum mesh working electrode, a platinum wire counter electrode, and a silver wire reference electrode in a 2 mm cell under a N_2 atmosphere.

Optical Spectroscopy. Ground-state absorption measurements were made on a Shimadzu UV-1601 spectrophotometer. The optical density of all samples was maintained between 0.3 and 0.6 at 532 nm ($\epsilon_{\text{PDI},545\text{nm}} = 46\,000\text{ M}^{-1}\text{ cm}^{-1}$)¹⁰¹ for both femtosecond and nanosecond transient absorption spectroscopy. Femtosecond transient absorption measurements were made using the 532 nm, 130 fs output from an optical parametric amplifier using techniques described earlier.¹⁰² Samples were placed in a 2 mm path length glass cuvette and sparged with nitrogen to prevent sample degradation. The samples were irradiated with 0.5–1.0 μJ per pulse focused to a 200 μm spot. The total instrument response function (IRF) for the pump–probe experiments was 180 fs. The three-dimensional data set of ΔA vs time (0–6 ns) and wavelength (440–800 nm) was subjected to singular value decomposition and global fitting to obtain the kinetic time constants and their decay-associated spectra using GlobalWorks software.¹⁰³

Samples for nanosecond transient absorption spectroscopy were placed in a 10 mm path length quartz cuvette equipped with a vacuum adapter and subjected to five freeze–pump–thaw degassing cycles. The samples were excited with 6 ns, 1 mJ, 545 nm laser pulses generated using the frequency-tripled output of a Continuum 8000 Nd:YAG laser to pump a Continuum Panther OPO. The excitation pulse was focused to a 5 mm diameter spot and matched to the diameter of the probe pulse generated using a xenon flashlamp (EG&G Electro-Optics FX-200). The signal was detected using a photomultiplier tube with high voltage applied to only four dynodes (Hamamatsu R928). The total instrument response time is 7 ns and is determined primarily by the laser pulse duration. Transient absorption kinetics were fit to a sum of exponentials with a Gaussian instrument function using Levenberg–Marquardt least-squares fitting.

EPR Spectroscopy. EPR measurements at both X-band (9.5 GHz) and W-band (94 GHz) were made using a Bruker Elexsys E680-X/W EPR spectrometer outfitted with a variable Q dielectric resonator (ER-4118X-MD5-W1) at X-band and a cylindrical resonator (EN-680-1021H) at W-band. For EPR measurements at the X-band, toluene solutions of **1–3** ($\sim 10^{-4}$ M) were loaded into quartz tubes (4 mm o.d. \times 2 mm i.d.), subjected to five freeze–pump–thaw degassing cycles on a vacuum line (10^{-4} mbar), and sealed using a hydrogen torch. For EPR measurements at W-band, samples of **1–3** ($\sim 10^{-4}$ M) were loaded into quartz tubes (0.84 mm o.d. \times 0.6 mm i.d.) in a N_2 -filled glovebox to a height of ~ 8 mm and sealed with a clear ridged UV doming epoxy (Epoxies, Etc., DC-7160 UV). The EPR samples were stored in a freezer in the dark when not being used.

Steady-state CW EPR spectra were measured at X-band using 0.2–2 mW microwave power and 0.01–0.05 mT field modulation at 100 KHz. All TREPR measurements were made at W-band. The samples were photoexcited at 532 nm (0.2 mJ/pulse, 7 ns, 10 Hz) using the frequency doubled output from a Nd:YAG laser (Quanta-Ray DCR-2) coupled to a fiber optic sample holder (Bruker E-600-1023 L). Following photoexcitation, kinetic traces of the transient magnetization were accumulated under CW microwave irradiation (6–20 mW) with the field modulation disabled. Microwave signals in emission (e) and/or enhanced absorption (a) were detected in both the real and the imaginary channels (quadrature detection) and amplified (20 MHz bandwidth, 10–90% risetime of 20 ns) to achieve a $Q/\pi \approx 30$ ns instrument response function (IRF), where Q is the quality factor of the resonator and ν is the resonant frequency. Sweeping the magnetic field gave 2D spectra versus both time and magnetic field. For each kinetic trace, the signal acquired prior to the laser pulse was subtracted from the data. Kinetic traces recorded at magnetic field values off resonance were considered background signals, whose average was subtracted from all kinetic traces. The spectra were subsequently phased into a Lorentzian part and a dispersive part, and the former, also known as the imaginary magnetic susceptibility χ'' , is presented.

Results

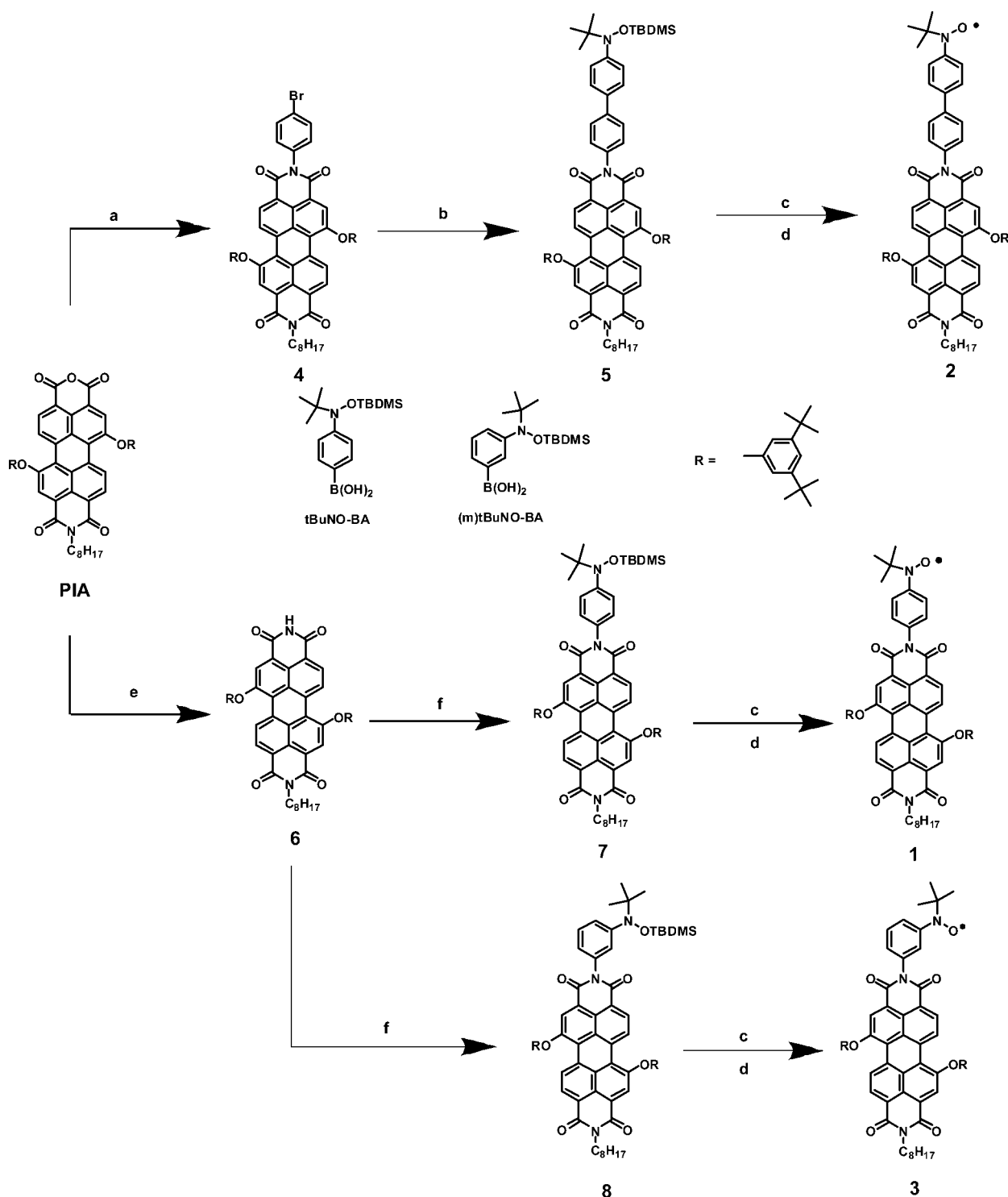
Synthesis and Steady-State Characterization. The synthesis of compounds **1–3** is summarized in Scheme 1, and the details are given in the Supporting Information. Briefly, the synthesis of ${}^2\text{BPNO}^{\bullet}$ -substituted PDI derivatives is carried out by first converting *N*-(*n*-octyl)perylene monoimide-monoanhydride (PIA)¹⁰¹ to *N*-(*n*-octyl)perylene diimide using urea in refluxing DMF. Copper-promoted coupling¹⁰⁴ of the resultant diimides with either the para or the meta boronic acid of the TBDMS-protected phenylnitroxide^{105,106} followed by deprotection of the

(102) Ahrens, M. J.; Sinks, L. E.; Rytchinski, B.; Liu, W. H.; Jones, B. A.; Giaimo, J. M.; Gusev, A. V.; Goshe, A. J.; Tiede, D. M.; Wasielewski, M. R. *J. Am. Chem. Soc.* **2004**, *126*, 8284–8294.
 (103) GlobalWorks; Olis, Inc.: Bogart, GA, 2008.

(104) Chernick, E. T.; Ahrens, M. J.; Scheidt, K. A.; Wasielewski, M. R. *J. Org. Chem.* **2005**, *70*, 1486–1489.

(105) Baskett, M.; Lahti, P. M. *Polyhedron* **2005**, *24*, 2645–2652.

(106) Lahti, P. M.; Liao, Y.; Julier, M.; Palacio, F. *Synth. Met.* **2001**, *122*, 485–493.

Scheme 1^a

^a (a) 4-Bromoaniline, pyridine, reflux, 96%; (b) *t*BuNO-BA, Pd(PPh₃)₄, Na₂CO₃, toluene/H₂O, 80 °C, 12 h, 60%; (c) TBAF, THF, 0 °C, 1–2 h; (d) PbO₂, toluene, RT, 1 h; (e) urea, DMF, reflux, 24 h, 45%; (f) *t*BuNO-BA(*m*)*t*BuNO-BA, Cu(OAc)₂, NEt₃, O₂, CH₂Cl₂, reflux, 48 h.

alcohol with TBAF and oxidation with lead dioxide results in the formation of **1** and **3**. The corresponding synthesis of **2** is carried out by condensing PIA with 4-bromoaniline, followed by a Suzuki cross-coupling of the resultant 4-bromophenyl imide with the para boronic acid of the TBDMS-protected phenylimide. Subsequent deprotection of the alcohol with TBAF and its oxidation with lead dioxide yields **2**.

Figure 1 shows the UV–vis absorption spectra for molecules **1**–**3**. PDI has a strong absorption at 545 nm ($\epsilon = 46\,000\text{ M}^{-1}$

cm^{-1}),¹⁰¹ which does not change significantly in **1**–**3**, indicating that the electronic coupling between PDI and the nitroxide radical is relatively weak. There is also an absorption feature in **1**–**3** between 300 and 350 nm due to absorption of ²BPNO[•], which is accentuated by a contribution from the additional phenyl in **2**. The UV–vis spectra of PDI and *p*-phenyl-²BPNO[•] alone are shown in Figure S1 (Supporting Information). ²BPNO[•]

(107) Weller, A. Z. Phys. Chem. 1982, 133, 93–98.

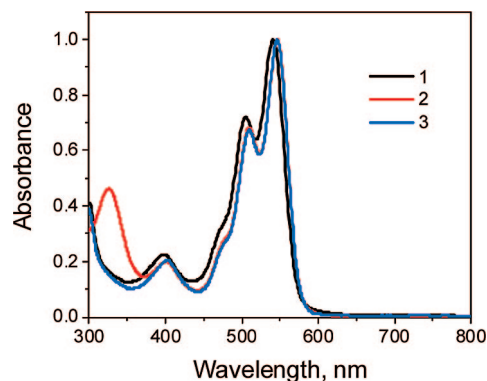


Figure 1. UV-vis spectra of compounds 1–3 in toluene solution.

Table 1. Redox Potentials and Free Energies of Charge Separation and Recombination for the Reaction ${}^2\text{BPNO}^{\bullet} + {}^1\text{PDI} \rightarrow \text{BPNO}^+ + \text{PDI}^{\bullet-}$ (V vs saturated calomel electrode (SCE))^a

molecule	E_{ox}^a	E_{red1}^a	E_{red2}^a	$-\Delta G_{\text{CS}}$		$-\Delta G_{\text{CR}}$	
				toluene	THF	toluene	THF
PDI		−0.61	−0.85				
${}^2\text{BPNO}^{\bullet}$	0.82	−1.25					
1	0.93	−0.66	−0.86	0.00	−0.50	2.23	1.73
2	0.83	−0.72	−0.93	0.11	−0.49	2.34	1.74
3	0.95	−0.68	−0.89	−0.05	−0.51	2.18	1.72

^a Measured in CH_2Cl_2 with 0.1 M tetra-*n*-butylammonium hexafluorophosphate with a ferrocene internal reference.

has a very weak absorption with a maximum at 475 nm that is typical of the n, π^* transition of nitroxide radicals.⁷² The PDI chromophore is normally highly fluorescent (see Figure S1 (Supporting Information), $\Phi_{\text{F}} = 0.98$);¹⁰¹ however, its fluorescence is almost completely quenched in **1–3**.

The one-electron redox potentials of **1–3** were obtained using cyclic voltammetry (Table 1). ${}^2\text{BPNO}^{\bullet}$ itself undergoes reversible oxidation and reduction at 0.82 and -1.25 V vs SCE, respectively. Spectroelectrochemistry shows that one-electron reduction of **1–3** produces $\text{PDI}^{\bullet-}$ (shown for **2** in Figure S2 (Supporting Information)), which displays a sharp feature at 720 nm, while one-electron oxidation shows no distinct absorption features between 400–800 nm associated with the oxidation of the radical. The free energies of the hypothetical charge separation and recombination reactions involving oxidation of ${}^2\text{BPNO}^{\bullet}$ by ${}^1\text{PDI}$, calculated using the Weller formalism¹⁰⁷ (Supporting Information), are also given in Table 1.

Transient Absorption Spectroscopy. The ultrafast excited-state dynamics of molecules **1–3** in both toluene and THF were studied using femtosecond transient absorption spectroscopy. The transient spectra are summarized in Figures 2 (toluene) and S3 (THF; Supporting Information). Photoexcitation of the PDI chromophore in **1–3** with a 532 nm, 130 fs laser pulse results in bleaching of the ground-state absorption band of PDI at 545 nm that occurs within the instrument response function (IRF) of the laser, as well as the appearance of a stimulated emission feature near 615 nm, an absorption band with a maximum near 700 nm, and broad absorption features between 450 and 775 nm that persist >6 ns. It is well known that ${}^1\text{PDI}$, ${}^3\text{PDI}$, and $\text{PDI}^{\bullet-}$ all have absorption features in the 700–750 nm wavelength region.^{100,101,108,109} The transient spectra for **1–3** between

450 and 775 nm and 0 and 6 ns in both toluene and THF were subjected to singular value decomposition and global fitting to obtain the principal kinetic components and their decay associated spectra, Figures 2 and S3 (Supporting Information). Each transient data set can be fit to two exponential decay components, a major component associated with the transient spectrum of ${}^1\text{PDI}$ including its prominent stimulated emission feature near 615 nm and a second minor component that lives $\gg 6$ ns. The decay-associated spectrum of this long-lived species is consistent with the known spectra and extinction coefficients of ${}^3\text{PDI}$.⁹¹ Nanosecond transient absorption spectroscopy was used to confirm this assignment (Figures 3 and S4 (Supporting Information)). For **1–3** in both toluene and THF, the ${}^3\text{PDI}$ transient spectral features appear at 480 nm with time constants (τ_{R}) that are very similar to those of the ultrafast ${}^1\text{PDI}$ decay component (τ_{D1}), while ${}^3\text{PDI}$ decays (τ_{D2}) on the order of microseconds (Table 2).

Using the decay-associated spectra, triplet yields (Table 2) were calculated from the ratio $\Delta A_{480\text{nm}}({}^3\text{PDI}) \cdot \epsilon_{505\text{nm}} / \Delta A_{505\text{nm}}({}^1\text{PDI}) \cdot (\epsilon'_{480\text{nm}} - \epsilon_{480\text{nm}})$, where $\epsilon_{505\text{nm}}$ and $\epsilon_{480\text{nm}}$ are the extinction coefficients of the PDI ground state at 505 nm ($3.2 \times 10^4 \text{ M}^{-1} \text{ cm}^{-1}$) and 480 nm ($1.5 \times 10^4 \text{ M}^{-1} \text{ cm}^{-1}$),¹⁰¹ while $\epsilon'_{480\text{nm}}$ is the extinction coefficient of ${}^3\text{PDI}$ at 480 nm ($4.0 \times 10^4 \text{ M}^{-1} \text{ cm}^{-1}$).⁹¹

EPR Spectroscopy. The steady-state EPR spectra of **1–3** consist of a dominant triplet centered at $g = 2.0057$ (Figure 4). This triplet is due to the large hyperfine splitting of the nitroxide ${}^{14}\text{N}$ nucleus, while the smaller splittings are due to the protons on the ring attached to it. The hyperfine splittings for **1–3** are listed in Table 3 and were obtained from simulations of the spectra using WINSIM.¹¹⁰ Additional lines observed for **2** (Figure 4) are due to very small hyperfine splittings (0.02 mT) resulting from protons on the second phenyl group that are ortho to the point at which ${}^2\text{BPNO}^{\bullet}$ is attached. In all three molecules spin leakage into the PDI chromophore is small, so that no hyperfine splittings due to the nitrogens and protons within PDI are observed.

TREPR spectra of **1** at W-band, shown in Figure 4, reveal an initial strongly emissive feature (Q) at 3369.3 mT ($g = 2.0040$) and a weaker emissive feature (D_1) at 3372.0 mT ($g = 2.0025$), which appear within the 30 ns IRF of the spectrometer following a 532 nm, 7 ns laser pulse at room temperature. A third emissive signal (D_0) with a hyperfine splitting of $a_{\text{N}} = 1.2$ mT characteristic of the nitrogen in ${}^2\text{BPNO}^{\bullet}$ appears at 3366.5 mT ($g = 2.0057$) with a somewhat slower time constant $\tau_1 = 120 \pm 20$ ns. At 260 ns, the Q signal is also split into a triplet with $a_{\text{N}} = 0.4$ mT. Each signal evolves in time from emissive to absorptive polarization, which ultimately decays (Figure S5 (Supporting Information) and Table 4). Similar behavior is observed following photoexcitation of **2**, in which the signals labeled Q and D_1 exhibit emissive polarization and evolve to absorptive polarization at longer times, while the signal attributed to ${}^2\text{BPNO}^{\bullet}$ remains emissive over the course of the experiment. The kinetics of all three signals are slower than those observed for **1**. The same three signals appear in the TREPR W-band data for **3** except that the initial polarization of all three signals is absorptive and evolves into emissive polarization, which is opposite to those for **1** and **2**. The kinetics for all three signals in **3** are similar in

(108) Rybchinski, B.; Sinks, L. E.; Wasielewski, M. R. *J. Phys. Chem. A* **2004**, *108*, 7497–7505.

(109) Rachford, A. A.; Goeb, S.; Castellano, F. N. *J. Am. Chem. Soc.* **2008**, *130*, 2766–2767.

(110) Duling, D. R. *J. Magn. Reson. B* **1994**, *104*, 105–110.

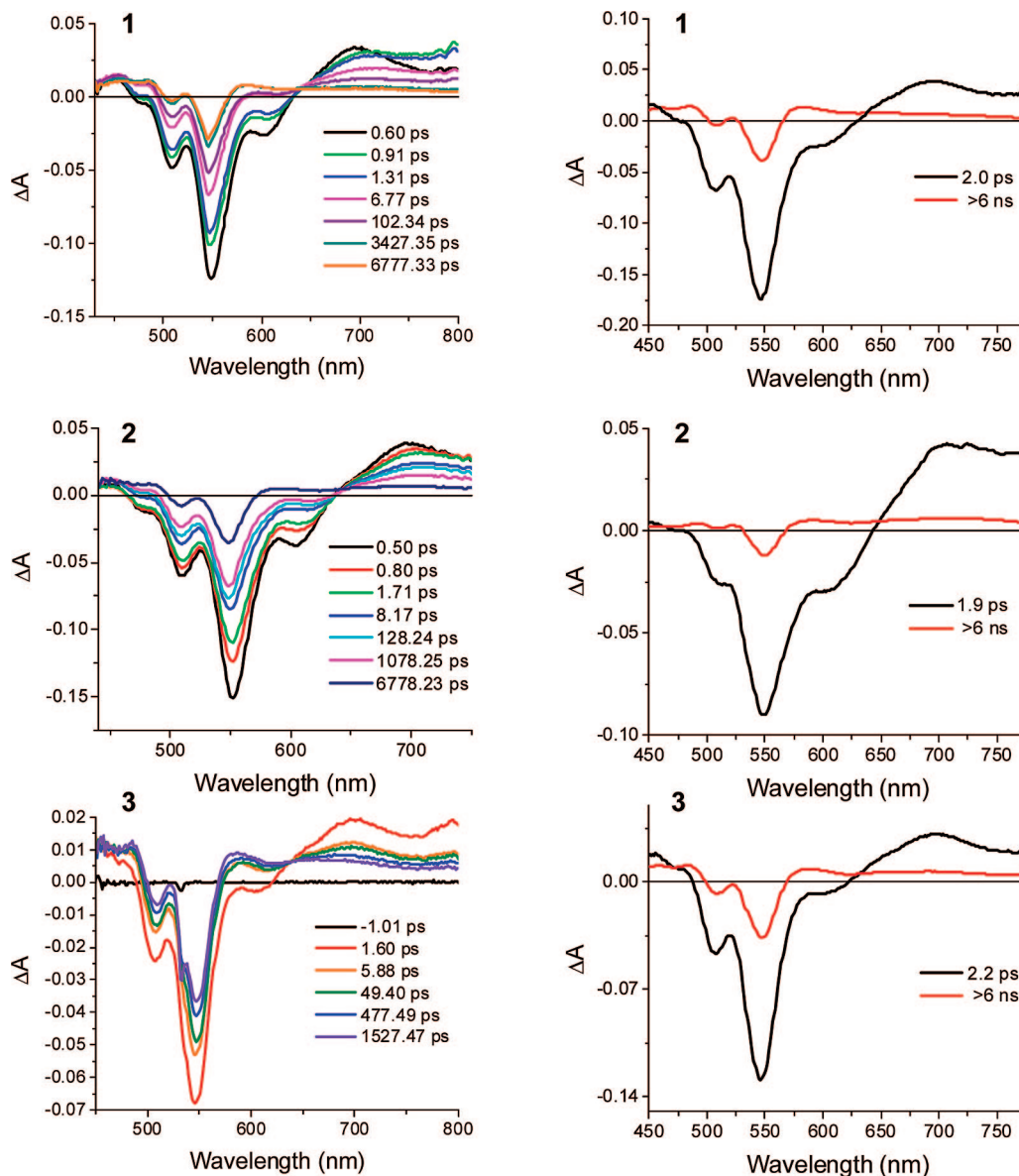


Figure 2. (Left) Transient absorption spectra of compounds **1–3** in toluene solution at the indicated times following a 130 fs, 532 nm laser pulse. (Right) Decay-associated spectra and their respective time constants for compounds **1–3** obtained by global analysis of the transient absorption data.

Table 2. Transient Absorption Species Associated Kinetics for **1–3** at 295 K

compound	τ_{D1} (ps), ^1PDI	τ_R (ps), ^3PDI	τ_{D2} (μs), ^3PDI	ϕ_T
1 (TOL)	2.0 ± 0.2	2.0 ± 0.2	0.54 ± 0.01	0.24 ± 0.02
1 (THF)	2.3 ± 0.2	2.4 ± 0.2	0.35 ± 0.01	0.23 ± 0.02
2 (TOL)	1.9 ± 0.2	2.0 ± 0.2	8.4 ± 0.5	0.12 ± 0.02
2 (THF)	2.1 ± 0.2	2.2 ± 0.2	4.5 ± 0.5	0.08 ± 0.02
3 (TOL)	2.2 ± 0.3	2.7 ± 0.3	0.80 ± 0.01	0.29 ± 0.02
3 (THF)	2.4 ± 0.3	3.0 ± 0.3	0.44 ± 0.01	0.31 ± 0.02

magnitude to those for **1** with the exception of τ_3 for D_0 , which is not observed (Table 4).

Discussion

Ultrafast Excited-State Dynamics. The femtosecond transient absorption spectra and kinetics of **1–3** show that ^1PDI decays very rapidly in the presence of $^2\text{BPNO}^*$ compared to its intrinsic 4.5 ns lifetime.¹⁰¹ As noted above, this rapid decay could be a consequence of any or all of the mechanisms outlined in eqs

1–4: electron transfer, energy transfer, EISC, or EIC. We modified the $\text{PDI}-^2\text{BPNO}^*$ distance, orientation (para vs meta), and solvent polarity for **1–3** to aid in determining the relative contributions of these mechanisms to the overall quenching of ^1PDI . Changing the distance and orientation of the nitroxide group relative to its point of attachment to PDI changes the electronic coupling between these two species, while varying the solvent polarity probes the role of electron transfer as a quenching mechanism.

The data in Table 1 show that electron transfer from $^2\text{BPNO}^*$ to ^1PDI in **1–3** is energetically unfavorable in toluene ($\Delta G_{CS} \cong 0$ eV), whereas it is strongly favored in THF ($\Delta G_{CS} \cong -0.5$ eV). These free energies of reaction predict that there should be a strong solvent dependence in the observed transient kinetics for both ^1PDI decay at 615 nm and for the formation and decay of PDI^* at 700 nm, if electron transfer occurs with a significant quantum yield. The kinetic data in Table 2 reveal no significant changes between toluene and THF. Given that the charge separation reaction should be in the normal region of the Marcus

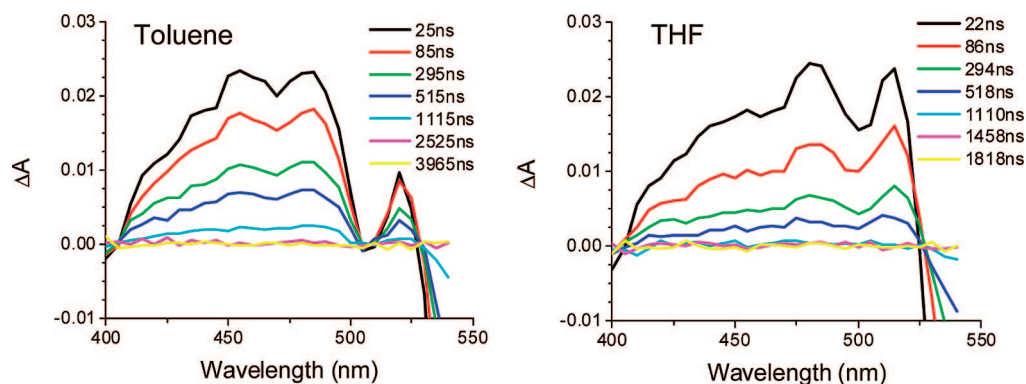


Figure 3. Transient absorption spectra of compound **1** in toluene and THF solutions at the indicated times following a 7 ns, 545 nm laser pulse.

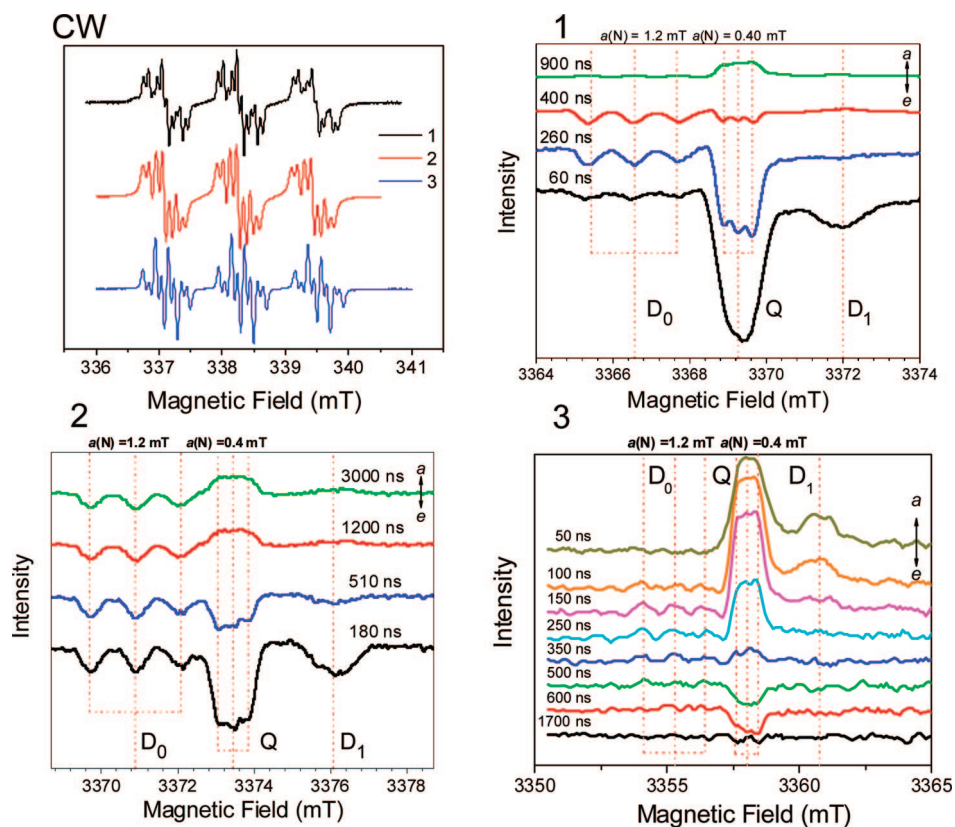


Figure 4. CW EPR spectra at X-band and W-band TREPR spectra of compounds **1–3** in toluene solution following a 7 ns, 532 nm laser pulse. All spectra are obtained at 295 K.

rate vs free energy curve,¹¹¹ a relatively large solvent effect is expected. Similarly, charge recombination should occur in the Marcus inverted region, which implies that the charge recombination reaction rates as indicated by the kinetics at 700 nm should be substantially faster in THF. Neither kinetic component observed at 700 nm shows this behavior, indicating that charge separation and recombination do not occur competitively with the other photophysical processes in **1–3**.

Energy transfer from ^1PDI to $^2\text{BPNO}^*$ is another possible quenching mechanism. The rate constant for FRET by the Förster dipole–dipole mechanism depends on the spectral overlap between the emission of the donor and the absorption of the acceptor (eq S1; Supporting Information).⁸⁸ Figure S1 (Supporting Information) shows that the very weak n,π^*

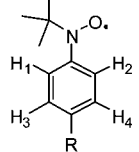
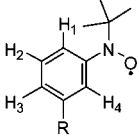
absorption of $^2\text{BPNO}^*$ overlaps poorly with the PDI fluorescence emission band. The PDI fluorescence slightly red shifts and becomes broader in more polar solvents; however, the absorbance of $^2\text{BPNO}^*$ is not affected by changes in solvent polarity, so that the overlap diminishes. The FRET time constants and efficiencies for **1–3** can be estimated from the $^2\text{BPNO}^*$ –PDI distance, r , and eqs S2 and S3 (Supporting Information) (Table 5). The calculated FRET time constants are much slower than the experimental time constants for ^1PDI decay (Table 2), so that it is unlikely that Förster energy transfer is responsible for the observed ultrafast quenching of ^1PDI in **1–3**.

Considering Dexter-type electron exchange driven energy transfer,¹¹² the rate of this process does not explicitly depend on the absorptivity of the acceptor, but it does depend on spectral

(111) Marcus, R. A. *J. Chem. Phys.* **1956**, *24*, 966–978.

(112) Dexter, D. L. *J. Chem. Phys.* **1953**, *21*, 836–850.

Table 3. EPR Hyperfine Couplings (mT)

	Molecule	a_N	a_1	a_2	a_3	a_4
	1	1.187	0.214	0.214	0.082	0.082
	2^a	1.185	0.211	0.211	0.094	0.094
	3	1.242	0.185	0.086	0.200	0.217

^a Additional splittings (0.02 mT, 2H) are observed.

Table 4. TREPR Kinetics in Toluene at 295 K

compound	Q ($g = 2.0040$)		D_1 ($g = 2.0025$)		D_0 ($g = 2.0057$)		
	τ_1 (ns)	τ_2 (ns)	τ_1 (ns)	τ_2 (ns)	τ_1 (ns)	τ_2 (ns)	τ_3 (ns)
1	140 ± 10	410 ± 10	46 ± 10	620 ± 90	120 ± 20	170 ± 30	>2000
2	210 ± 10	>3000	200 ± 10	>3000	200 ± 60	>3000	
3	150 ± 10	740 ± 30	32 ± 8	800 ± 400	110 ± 10	350 ± 30	

Table 5. Estimated Förster FRET Time Constants and Efficiencies^a

compound	r (Å)	toluene		THF	
		τ_{ENT} (ps)	ϕ_{ENT} (%)	τ_{ENT} (ps)	ϕ_{ENT} (%)
1	11.4	54	99	67	99
2	15.7	360	93	455	91
3	10.0	32	99	40	99

^a Calculated using PhotochemCAD 2.1 as described in the Supporting Information.

overlap, so that the poor overlap between the PDI emission and ²BPNO* absorption spectra discussed above necessarily make Dexter energy transfer slow for **1–3** as well. Moreover, energy transfer requires that the energy of the excited doublet state ²BPNO* (~2.4 eV) is below that of ¹*PDI (2.23 eV), which is not the case. Thus, the requirements for ultrafast, efficient energy transfer from ¹*PDI to ²BPNO* are not met for **1–3**, so that it is unlikely this mechanism can account for the ultrafast decay of ¹*PDI. In fact, only one conclusive example of energy transfer from an emitting chromophore to a nitroxide radical has been previously reported,⁸⁷ which is likely due to the very low extinction coefficients of most nitroxide radicals in the visible.⁷²

The positive transient absorption changes observed near 700 nm may have contributions from ¹*PDI, ³*PDI, and/or PDI⁻, while those observed near 480 nm are due largely to ³*PDI.⁹¹ The decay of ¹*PDI is accompanied by ultrafast formation of ³*PDI with yields ranging from 0.08 to 0.31, as indicated by the formation of the ³*PDI transient spectrum with time constants probed at 480 nm comparable to those for the decay-associated spectrum of ¹*PDI. Normally, the yield of ³*PDI produced by SO-ISC is <0.01, as indicated by the near unity quantum yield of PDI fluorescence. Higher yields of ³*PDI have been observed using triplet sensitizers and heavy atom effects of metal

complexes attached to PDI.^{26,91,109,113,114} In addition, a variety of electron donor–acceptor systems in which PDI acts as an electron acceptor have allowed access to ³*PDI by radical pair intersystem crossing, followed by charge recombination of the triplet radical pair. The yields of ³*PDI vary widely in these systems and depend on the yields of the precursor radical pair states.^{26,113,114}

The ultrafast formation of ³*PDI from ¹*PDI is most likely due to the EISC mechanism.⁸⁹ In this mechanism ²BPNO* mixes with ¹*PDI to produce an excited state with an overall doublet multiplicity (D_2); similarly, ²BPNO* mixes with ³*PDI resulting in states having both doublet (D_1) and quartet (Q) multiplicities, Figure 5. Note that the three-spin D_1 and Q states both have two unpaired electrons on PDI, so that their optical transient absorption spectra are indistinguishable from that of ³*PDI. The electron exchange interaction between ¹*PDI and ²BPNO* serves as the first-order perturbation that drives EISC. The magnitude of this perturbation, and thus the overall intersystem crossing rate, depends strongly on the electronic overlap between the orbitals that contribute to ¹*PDI and the singly occupied molecular orbital (SOMO) of ²BPNO*. Increasing the distance between ²BPNO* and ¹*PDI should diminish this overlap and result in an overall reduction in the yield of ³*PDI (i.e., D_1 and Q). Comparing the data for **1** and **2** in toluene, a 4.3 Å increase in the distance between the radical and the chromophore results in about a factor of 2 decrease in ³*PDI yield. In molecule **1**, the spin density at the 4-position of ²BPNO* is about 0.1,¹¹⁵ which further delocalizes into the adjacent phenyl ring in **2**. This places enough π spin density within the phenyl ring attached to PDI to produce sufficient electronic coupling between the radical and ¹*PDI to drive ultrafast EISC. Placing

(113) Ahrens, M. J.; Kelley, R. F.; Dance, Z. E. X.; Wasielewski, M. R. *Phys. Chem. Chem. Phys.* **2007**, *9*, 1469–1478.

(114) Prodi, A.; Chiaboli, C.; Scandola, F.; Iengo, E.; Alessio, E.; Dobrawa, R.; Würthner, F. *J. Am. Chem. Soc.* **2005**, *127*, 1454–1462.

(115) Shultz, D. A.; Gwaltney, K. P.; Lee, H. *J. Org. Chem.* **1998**, *63*, 769–774.

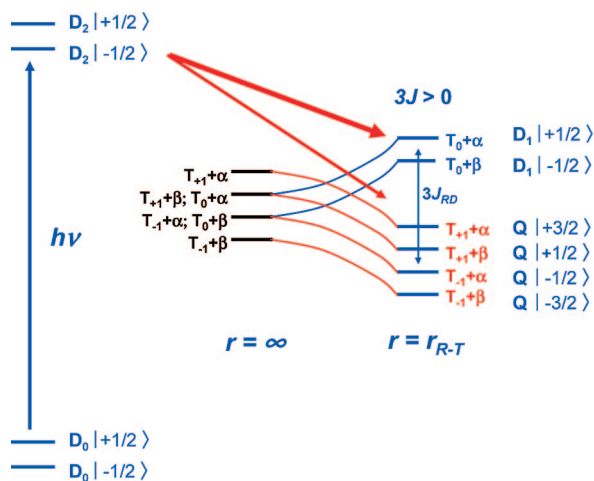


Figure 5. Energy levels created after doublet–triplet mixing. $D_2 \rightarrow D_1$ internal conversion is more rapid (thick red arrow) than $D_2 \rightarrow Q$ intersystem crossing (thin red arrow). The levels shown are for $3J > 0$.

${}^2\text{BPNO}^*$ in a meta orientation relative to PDI, as in **3**, decreases the π spin density at the carbon atom at which ${}^2\text{BPNO}^*$ is attached to PDI, thereby reducing the overall π -electron coupling between ${}^2\text{BPNO}^*$ and ${}^1\text{PDI}$. However, the measured quantum yields of ${}^3\text{PDI}$ for **3** in both toluene and THF solution are about 25% higher than those for **1**, so that other pathways to enhance the electronic coupling between ${}^2\text{BPNO}^*$ and ${}^1\text{PDI}$ must be operative. In addition to the through-bond π interaction, the spin of the unpaired electron on the oxygen atom of the nitroxide can also delocalize through the σ -bond framework by a spin polarization mechanism.^{116,117} As a consequence, the shorter σ pathway between ${}^2\text{BPNO}^*$ and ${}^1\text{PDI}$ in **3** relative to **1** may enhance the coupling between them.

Given that EISC is driven by a first-order perturbation, the energy gap between ${}^1\text{PDI}$ and ${}^3\text{PDI}$ is also important. Since the energy gap between these two states is about 1.2 eV,⁹¹ one might expect that EISC would be slower than observed. However, semiempirical ZINDO/S calculations¹¹⁸ place the T_2 state of PDI (${}^3\text{PDI}$) nearly isoenergetic with ${}^1\text{PDI}$. This makes it more likely that EISC occurs between ${}^1\text{PDI}$ and ${}^3\text{PDI}$, followed by very rapid internal conversion from ${}^3\text{PDI}$ to ${}^3\text{PDI}$. The states resulting from mixing ${}^3\text{PDI}$ and ${}^2\text{BPNO}^*$ are not shown in Figure 5, but their initial spin configurations would be carried over to D_1 and Q shown in the figure because of the ultrafast nature of this internal conversion process.

The ${}^3\text{PDI}$ lifetimes of **1–3** observed by nanosecond transient absorption spectroscopy are all substantially shorter than the intrinsic ${}^3\text{PDI}$ lifetime of 100 μs ⁹¹ and display only small solvent effects. The nanosecond transient spectra show no evidence for electron transfer from the triplet state to yield $\text{BPNO}^+-\text{PDI}^-$, which is reasonable given that the energy of ${}^3\text{PDI}$ is only 1.2 eV,⁹¹ so that even in polar solvents $\Delta G_{\text{CS}} > 0$. The 2-fold change in ${}^3\text{PDI}$ lifetime as a function of solvent is most likely a result of a small change in nonradiative rate of ${}^3\text{PDI}$. The ${}^3\text{PDI}$ lifetimes of **1–3** will be discussed further in the context of the TREPR kinetics presented below.

Since the ${}^3\text{PDI}$ yields for **1–3** are all ≤ 0.31 , ultrafast electron exchange driven EIC also rapidly returns ${}^1\text{PDI}$ to the ground

state. This process is due to enhanced vibrational relaxation as has been discussed earlier.^{72,119}

Time-Resolved EPR. Photoexcitation of the formally doublet ground-state D_0 produces the excited-state D_2 in which the two electrons confined to PDI are spin paired (Figure 5). Our transient optical absorption data show that EISC occurs in ~ 2 ps in **1–3**, which is much faster than typical SO-ISC (e.g., the rate for ${}^1\text{PDI} \rightarrow {}^3\text{PDI}$ is only $\sim 10^6 \text{ s}^{-1}$), so that this ultrafast process is most likely driven by the exchange interactions between each of the two spin-paired electrons in ${}^1\text{PDI}$ and the unpaired electron on ${}^2\text{BPNO}^*$.⁸⁹ The resulting three-spin system is best described at high magnetic fields by mixing the T_{+1} , T_0 , and T_{-1} eigenstates of ${}^3\text{PDI}$ with the α and β spin states of ${}^2\text{BPNO}^*$ to yield excited doublet (D_1) and quartet (Q) states (Figure 5). Transitions from the spin sublevels of D_2 to those of D_1 (Figure 5, thick red arrow) are partially allowed because the initial and final state have the same overall multiplicity, whereas the transitions from the spin sublevels of D_2 to Q (Figure 5, thin red arrow) involve a change in multiplicity, so that they are formally forbidden. Therefore, the $D_2 \rightarrow D_1$ transition is expected to be more rapid than the $D_2 \rightarrow Q$ transition, resulting in a larger initial population of D_1 relative to that of Q . Following the formation of D_1 and Q , the applied microwave field induces transitions between the $\Delta m_s = \pm 1$ levels within the D_1 , Q , and D_0 manifolds.

The conventional RTPM^{22,43–56} spin polarization mechanism derived from the three-spin interaction of an excited-state chromophore and a radical requires that the two species interact in a diffusive encounter. The chromophore–radical distances and the electronic coupling between the chromophore and the radical in **1–3** are controlled using rigid covalent linkages, so that the RTPM mechanism of CIDEP is precluded. The alternative ESPT mechanism requires the polarized triplet state of the chromophore to transfer its polarization to the radical and is thought to occur through either direct spin exchange¹²⁰ or energy transfer.¹²¹ Direct spin exchange is ruled out because it requires the initial polarization of ${}^2\text{BPNO}^*$ to be the same in both **1** and **3**, whereas the observed initial polarization of ${}^2\text{BPNO}^*$ in **1** is opposite to that in **3**. Energy transfer is ruled out for reasons already given.

The TREPR spectra of **1–3** at W-band all show a spin-polarized signal centered at $g = 2.0057$ (Figure 4), which is split into three lines having the same hyperfine coupling to ${}^{14}\text{N}$ as does the ground-state signal of ${}^2\text{BPNO}^*$ and is thus assigned to that radical. If the exchange interaction is much larger than the Zeeman interaction that splits the spin sublevels ($3J \gg g\beta B_0$, Figure 5), the D_1 and Q states can be adequately described by separate spin Hamiltonians.¹²² The measured exchange interaction between two ${}^2\text{BPNO}^*$ radicals appended to the same carbon atom of an ethylene spacer is $J = -24 \text{ cm}^{-1}$,¹²³ whereas replacing the ethylene with a meta-phenyl spacer yields $J = -4 \text{ cm}^{-1}$.¹²⁴ The ${}^3\text{PDI}$ – ${}^2\text{BPNO}^*$ distances and number of bonds joining them in **1–3** are comparable to those in the ${}^2\text{BPNO}^*$ biradical with the ethylene spacer, so that we expect that J

(116) McConnell, H. M.; Chesnut, D. B. *J. Chem. Phys.* **1958**, *28*, 107–117.

(117) Colpa, J. P.; de Boer, E. *Mol. Phys.* **1964**, *7*, 333–348.

(118) *Hyperchem*; Hypercube Inc.: Gainesville, Florida.

(119) Braun, A. M.; Hammond, W. B.; Cassidy, H. G. *J. Am. Chem. Soc.* **1969**, *91*, 6196–6197.

(120) Obi, K.; Imamura, T. *Rev. Chem. Intern.* **1986**, *7*, 225–242.

(121) Jenks, W. S.; Turro, N. J. *Res. Chem. Intermed.* **1990**, *13*, 237–300.

(122) Bencini, A.; Gatteschi, D. *Electron paramagnetic resonance of exchange coupled systems*; Springer-Verlag: Berlin, New York, 1990.

(123) Shultz, D. A.; Boal, A. K.; Lee, H.; Farmer, G. T. *J. Org. Chem.* **1999**, *64*, 4386–4396.

(124) Kanno, F.; Inoue, K.; Koga, N.; Iwamura, H. *J. Phys. Chem.* **1993**, *97*, 13267–13272.

between the electrons on ^3PDI and $^2\text{BPNO}$ should also be comparable, thus making $|3J| \gg g\beta B_0$ ($\sim 3 \text{ cm}^{-1}$ at the W-band). Under this condition both the g factors and the hyperfine couplings exhibited by spin sublevel transitions within D_1 and Q can be approximated by¹²²

$$g_{D_1} = -\frac{1}{3}g_R + \frac{4}{3}g_T \quad (5)$$

$$a_{D_1}^N = -\frac{1}{3}a_R^N \quad (6)$$

$$g_Q = \frac{1}{3}g_R + \frac{2}{3}g_T \quad (7)$$

$$a_Q^N = \frac{1}{3}a_R^N \quad (8)$$

Using eqs 5 and 7 and the g factor of ^3PDI ($g = 2.0033$, measured independently from electron donor–acceptor systems in which ^3PDI is produced by charge recombination of spin-correlated radical pairs^{125,126}), the predicted g factors of the D_1 and Q states correspond very well to the observed signals at $g = 2.0025$ and 2.0040 , respectively. The three transitions expected from Q overlap strongly because of the small degree of anisotropy observed in the spectra. However, the observed signal for Q in **1–3** is split into a triplet for which $a_Q^N = 0.4 \text{ mT}$ as predicted by eq 8. Given the limitations of signal-to-noise and spectral line width, a_Q^N is not apparent at all times. In addition, the spectral line due to D_1 is lifetime broadened in **1–3**, so that $a_{D_1}^N$ is not observed. The ability of this approximate treatment to predict the g factors and hyperfine couplings of the observed D_1 and Q signals supports the assumption that $|3J| \gg g\beta B_0$.

For **1** and **2**, the TREPR spectra at early times show that all three signals due to D_0 , D_1 , and Q are initially polarized in emission, while for **3** all three signals are polarized in absorption. Even though D_1 and Q are well separated by $3J$, the zero-field splitting interaction, H_{ZFS} , of the two unpaired electrons localized on PDI mixes D_1 and Q

$$H_{ZFS} = D(S_z^2 - S^2/3) + E(S_x^2 - S_y^2) = D(S_z^2 - S^2/3) + E(S_+^2 + S_-^2)/2 \quad (9)$$

where D and E are the zero-field splitting parameters. Thus, the rate of intersystem crossing from the spin sublevels of D_1 to those of Q is given by

$$k(|D_1(m_S)\rangle \rightarrow |Q(m_S)\rangle) = k_0 \cdot FC \cdot \frac{| \langle Q(m_S) | H_{ZFS} | D_1(m_S) \rangle |^2}{(E_Q(m_S) - E_{D_1}(m_S))^2} \quad (10)$$

where k_0 is the fully spin-allowed, vibrationally limited rate constant ($\sim 10^{13} \text{ s}^{-1}$), FC is the Franck–Condon factor for the transition, and the final term is the spin-dependent transition strength resulting from the H_{ZFS} perturbation that mixes D_1 and Q . The Franck–Condon terms should be similar (and large) for all transitions because the energy gaps between the spin sublevels are all much smaller than those between typical vibronic transitions.

Referring to Figure 6a, the intersystem crossing rate for **1** and **2** is greatest for $|D_1(-1/2)\rangle \rightarrow |Q(+3/2)\rangle$ due to the fact that the energy gap between these states ($E_Q(+3/2) - E_{D_1}(-1/2)$) is the smallest for any of the six allowed ($\Delta m_S = \pm 1, \pm 2$)

transitions. Thus, intersystem crossing results in greater depletion of the $|D_1(-1/2)\rangle$ population relative to that of $|D_1(1/2)\rangle$ as indicated in Figure 6a. The remaining relative transition rates are also governed by eq 10, so that the relative sublevel populations of D_1 and Q are established prior to our IRF of $\sim 30 \text{ ns}$, as evidenced by the observed initial net emissive polarization of both the D_1 and Q signals. The emissive character of the signals from both D_1 and Q within **1** and **2** strongly support ferromagnetic ordering for these spin manifolds ($3J > 0$), as illustrated in Figures 5 and 6. In turn, the initially all absorptive signals observed for **3** are consistent with antiferromagnetic ordering ($3J < 0$). The change in the sign of the exchange interaction in going from a para to a meta substitution pattern in a benzene ring is consistent with spin polarization of electron density at the carbon atoms within the HOMOs and LUMOs of substituted benzenes.^{127,128} The TREPR spectra of these transitions at 295 K in toluene do not exhibit their full anisotropy because the molecules are tumbling faster than the time scale corresponding to the energy differences between the spin sublevels.

The $\sim 200 \text{ cm}^{-1}$ thermal energy at 295 K most likely exceeds $|3J|$ significantly, so that reverse intersystem crossing from Q to D_1 is fully competitive with the decay of these states to ground-state D_0 and relaxation of their spin populations back to a Boltzmann distribution. This reverse intersystem crossing has been termed the reverse quartet mechanism (RQM) and used to describe the TREPR spectra and kinetics of a tetramethylpiperidiny-*N*-oxyl (TEMPO) radical covalently bound to C_{60} .¹⁸ For molecules **1** and **2**, when $3J > 0$, the initial spin level populations of D_1 and Q (Figure 6a) evolve in time as the transitions from the spin sublevels of Q back to D_1 occur (Figure 6b). This redistribution of spin population within D_1 and Q coupled with the relative rates of depletion of the D_1 and Q populations to ground-state D_0 results in the observed absorptive TREPR transitions at later times. Focusing again on the two sublevels that are closest in energy (Figure 6b), for $|Q(+3/2)\rangle \rightarrow |D_1(-1/2)\rangle$ the relatively large initial population in $|Q(+3/2)\rangle$ that was derived from both $|D_1(-1/2)\rangle$ and $|D_1(+1/2)\rangle$ is returned preferentially to $|D_1(-1/2)\rangle$, once again due to the smaller gap between $|D_1(-1/2)\rangle$ and $|Q(+3/2)\rangle$. A similar qualitative analysis can be made for the remaining spin sublevels. The same mechanistic picture prevails for **3**, except that the spin manifold of Q is now energetically above that of D_1 (i.e., $3J < 0$), and the two states closest in energy are $|D_1(+1/2)\rangle$ and $|Q(-3/2)\rangle$.

The kinetics for the formation and decay of the spin-polarized TREPR signals of D_1 , Q , and D_0 are a complex mix of population changes between the spin sublevels and spin relaxation processes. This problem was initially treated using a modified Bloch equation approach including kinetic terms connecting the spin sublevels of D_1 and Q to those of the ground-state D_0 .¹⁸ This model yields a complex series of equations having many rate constants that are not readily accessible experimentally. Tarasov et al.^{58,59} recently applied

(125) Dance, Z. E. X.; Mickle, S. M.; Wilson, T. M.; Ricks, A. B.; Scott, A. M.; Ratner, M. A.; Wasielewski, M. R. *J. Phys. Chem. A* **2008**, *112*, 4194–4201.

(126) Zeidan, T. A.; Carmieli, R.; Kelley, R. F.; Wilson, T. M.; Lewis, F. D.; Wasielewski, M. R. *J. Am. Chem. Soc.* **2008**, *130*, 13945–13955.

(127) Thompson, A. L.; Ahn, T.-S.; Thomas, K. R. J.; Thayumanavan, S.; Martinez, T. J.; Bardeen, C. J. *J. Am. Chem. Soc.* **2005**, *127*, 16348–16349.

(128) Zimmerman, H. E. *J. Phys. Chem. A* **1998**, *102*, 5616–5621.

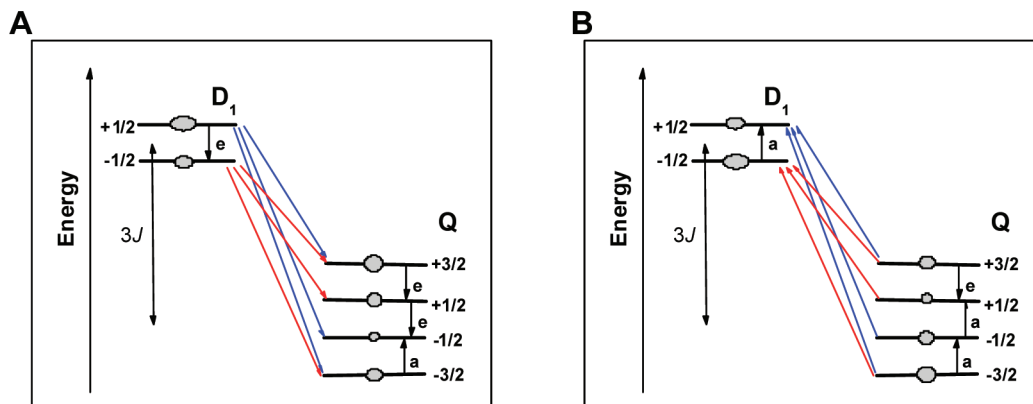


Figure 6. D_1 – Q intersystem crossing resulting in emissive polarization from D_1 and Q at (A) early times followed by enhanced absorption at (B) later times. The levels shown are for $3J > 0$.

the stochastic Liouville equation to this problem taking into account the relevant kinetic terms in the relaxation operator and considering the full anisotropy of the Zeeman and dipolar interactions. This elegant approach accounts for the case in which the three-spin system may be tumbling in solution at a rate that is comparable to the transition rates between the spin manifolds as well as the spin relaxation rates. This treatment successfully simulates the observed time-dependent inversion of the initial spin polarization of D_1 and Q within a Zn tetraphenylporphyrin coordinated to 3-pyridyl-*t*-Bu-nitroxide. The authors emphasized that the observed polarization inversion of both the D_1 and Q signals at later times is essentially a kinetic effect resulting from the competition between spin selective and nonselective transition rates.

Even though it is difficult to determine a complete set of rate constants experimentally at room temperature in fluid solution, a semiquantitative picture of the spin dynamics of these states within **1–3** can be obtained by examining the kinetic parameters that are observed. The appearance of the D_1 and Q TREPR signals in **1–3** all occur within the 30 ns IRF. The spin-allowed nature of the $D_2 \rightarrow D_1$ transitions relative to the $D_2 \rightarrow Q$ transitions results in overpopulation of D_1 . As discussed above, the subsequent transitions $D_1 \rightarrow Q$ leave $|D_1(+1/2)\rangle$ overpopulated in **1** and **2**, which results in an emissive D_1 signal. For molecule **1**, the decay of the D_1 signal from emission to absorption occurs very rapidly ($\tau_1 = 46$ ns), so that this decay monitors the sum of the rates of the allowed $D_1 \rightarrow Q$ transitions (Figure 6a) and those of $D_1 \rightarrow D_0$. The decay of the emissive Q signal ($\tau_1 = 140$ ns) largely reflects the sum of the rates of the $Q \rightarrow D_1$ transitions that repopulate D_1 (Figure 6b) and the $Q \rightarrow D_0$ transitions to ground state. The $Q \rightarrow D_1$ transitions should be faster than the $Q \rightarrow D_0$ transitions because the Q – D_0 energy gap is much larger than the Q – D_1 gap (cf. eq 10). The Q signal is much stronger than the D_1 signal because the transition probabilities between the spin sublevels of Q are about 4 times larger than those of D_1 .²² The D_0 signal that results from return of the system to the ground-state PDI–²BPNO* is polarized in the same sense as is D_1 and Q , yet appears with $\tau_1 = 120$ ns, which is slower than the IRF. The 120 ns appearance time constant for the emissive D_0 signal agrees within experimental uncertainty with the 140 ns decay of the emissive signal of Q , which is consistent with the overall rate of the appearance of the emissive D_0 signal being limited by repopulation of D_1 followed by rapid decay of the partially spin-allowed $D_1 \rightarrow D_0$ transitions. The corresponding $Q \rightarrow D_0$ intersystem crossing

transitions are slower than the $D_1 \rightarrow D_0$ transitions because of their spin-forbidden nature.

All of the subsequent absorptive signals for D_1 , Q , and D_0 in **1** and **2** have longer lifetimes than those of the emissive signals, which implies that their observed lifetimes may in fact be limited by spin relaxation. However, the data in Table 2 show that the lifetime of ³PDI ($\tau_{D_2} = 0.54 \mu\text{s}$) for **1** measured in toluene using nanosecond transient optical absorption agrees reasonably well with the time constants for the decay of the absorptive TREPR signal from D_1 ($\tau_2 = 620$ ns) and Q ($\tau_2 = 410$ ns), given the error bars on the TREPR kinetics. Since the optical kinetic measurements of ³PDI monitor the decay of the total D_1 and Q population and are not spin selective or sensitive to spin relaxation, the agreement between the kinetics determined by optical and TREPR techniques strongly suggests that spin relaxation contributes little to the overall measured TREPR kinetics.

A similar picture emerges upon examination of the TREPR kinetics for **3** except for the fact that since $3J < 0$, the energy ordering of D_1 and Q is reversed, and the temporal order of the absorptive and emissive transitions is inverted. Once again, the spin-allowed nature of the $D_2 \rightarrow D_1$ transitions relative to the $D_2 \rightarrow Q$ transitions results in overpopulation of D_1 . However, unlike the case of **1** and **2**, the subsequent $D_1 \rightarrow Q$ transitions leave $|D_1(-1/2)\rangle$, $|Q(-3/2)\rangle$, and $|Q(-1/2)\rangle$ overpopulated in **3**, which produces initially absorptive D_1 and Q signals. The absorptive signals from both D_1 ($\tau_1 = 32$ ns) and Q ($\tau_1 = 150$ ns) decay with the same time constants as the corresponding emissive signals of **1** within experimental uncertainty. In addition, the appearance time constant for D_0 ($\tau_1 = 110$ ns) is also the same as that of **1** within experimental uncertainty, which is once again consistent with the overall rate of the appearance of the emissive D_0 signal being limited by repopulation of D_1 followed by rapid decay of the spin-allowed $D_1 \rightarrow D_0$ transitions. The data in Table 2 show that the lifetime of ³PDI ($\tau_{D_2} = 0.80 \mu\text{s}$) measured in toluene using nanosecond transient optical absorption agrees very well with the time constants for the decay of the absorptive TREPR signal from D_1 ($\tau_2 = 800$ ns) and Q ($\tau_2 = 740$ ns). Thus, it is likely that the submicrosecond decay rates for these absorptive signals do not have significant contributions from spin relaxation. The much longer D_0 decay time constant of $\tau_3 > 2 \mu\text{s}$ that is apparent for **1** is no longer observed for **3** as a result of the lower signal intensity in **3**.

For molecule **2**, the time constants for the decay of the emissive D_1 ($\tau_1 = 200$ ns) and Q ($\tau_1 = 210$ ns) signals to their

respective absorptive signals, as well as the appearance of the emissive D_0 ($\tau_1 = 200$ ns) signal, are all the same within experimental uncertainty. The additional phenyl spacer in **2** should decrease $|3J|$ due to the increased distance between the two unpaired spins on PDI and ${}^2\text{BPNO}^*$ and decrease H_{ZFS} as a result of a small increase in the delocalization of the PDI unpaired electrons onto the phenyl bridge. According to eq 10, decreasing $|3J|$ reduces the energy gaps between the spin sublevels, which should increase the rates of the $D_1 \leftrightarrow Q$ transitions, while decreasing H_{ZFS} should decrease these rates. Our data suggest that changes in H_{ZFS} have slightly more influence on the measured rates because the decay times of the emissive signals for D_1 and Q are only about 4 and 1.5 times longer, respectively, than those of **1**. The overall slowing of the spin dynamics within **2** is reflected in the time constant for the decay of the initially emissive D_0 signal to the absorptive signal, which is also slow and does not invert during the observed $3 \mu\text{s}$ time window shown in Figure 4. The decay time constants of the absorptive D_1 and Q TREPR signals are $\tau_2 > 3 \mu\text{s}$, which is consistent with the ${}^3\text{PDI}$ lifetime of **2** ($\tau_{\text{D2}} = 8.4 \mu\text{s}$) measured in toluene using nanosecond transient optical absorption. At these long decay times, spin relaxation most likely contributes to the overall decay of D_0 measured by TREPR.

Finally, one aspect of the RQM mechanism originally proposed for the TEMPO– C_{60} system that does not apply to **1–3** relates to the relaxation of D_1 back to the ground-state D_0 . In the TEMPO– C_{60} system, electron transfer from TEMPO to C_{60} to produce a CT state followed by charge recombination leading to the ground state was proposed, $D_1 \rightarrow \text{CT} \rightarrow D_0$. In our systems, however, the energy of ${}^3\text{PDI}$ is only 1.2 eV,⁹¹ so that even in polar solvents, $\Delta G_{\text{CS}} > 0$, and electron transfer cannot occur.

Conclusions

Our results show that the ${}^2\text{BPNO}^*$ radical quenches ${}^1\text{PDI}$ exclusively by the EISC and EIC mechanisms with time

constants of $\tau \cong 2$ ps. Rapid photogeneration of the three-spin system results in the formation of excited doublet (D_1) and quartet (Q) states involving the strongly coupled unpaired electrons confined to PDI (i.e., ${}^3\text{PDI}$), which are each much more weakly coupled to the unpaired electron on ${}^2\text{BPNO}^*$. Attachment of ${}^2\text{BPNO}^*$ at its 4-position to the imide nitrogen atom of ${}^3\text{PDI}$ (**1**) or by means of an intervening *p*-phenylene group (**2**) results in ferromagnetic coupling ($3J > 0$) between the spins, while attachment of ${}^2\text{BPNO}^*$ at its 3-position to the imide nitrogen atom of ${}^3\text{PDI}$ (**3**) results in antiferromagnetic coupling ($3J < 0$) between the spins. Following photoexcitation of PDI and ultrafast EISC, the TREPR experiments at high magnetic fields provide sufficient spectral resolution to allow the observation of the dynamics of the spin-polarized D_1 and Q excited states as well as the spin-polarized ground-state of PDI– ${}^2\text{BPNO}^*$ (D_0). The rapid, photon-controlled formation of specific polarized spin states that can be achieved by tailoring the structure of the PDI–radical system gives us an important building block for assembling a variety of complex multispin molecular systems in which spin information can be transferred to specific sites within the systems. This type of behavior has potential uses in the development of new materials for organic spintronics.

Acknowledgment. This work was supported by the National Science Foundation, under Grant No. CHE-0718928, and by the MRSEC program of the NSF through the Northwestern MRSEC (DMR-0520513). The authors would also like to acknowledge Dr. Z. Dance and Dr. R. Carmieli for their assistance in the TREPR data collection. M.T.C. thanks the Link Foundation for a Fellowship.

Supporting Information Available: Experimental details, including synthesis and additional transient absorption and TREPR data. This material is available free of charge via the Internet at <http://pubs.acs.org>.

JA808924F